Journal of Photochemistry & Photobiology, A: Chemistry 444 (2023) 114970

Contents lists available at ScienceDirect

Journal of Photochemistry & Photobiology, A: Chemistry

journal homepage: www.elsevier.com/locate/jphotochem

Catalytic and antimicrobial properties of Ag and polyacrylic acid doped SrO nanocomposites; molecular docking analysis

Husnain Shahzad [a], Muhammad Imran [a,*], Ali Haider [b], Sadia Naz [c], Ehtisham Umar [d], Anwar Ul-Hamid [e,*], Walid Nabgan [f,*], Mohammed M. Algaradah [g], Ahmed M. Fouda [h], Junaid Haider [c], Muhammad Ikram [d,*]

[a] Department of Chemistry, Government College University, Faisalabad, Sahiwal Road, Sahiwal, Punjab, 57000, Pakistan
[b] Department of Clinical Sciences, Faculty of Veterinary and Animal Sciences, Muhammad Nawaz Shareef, University of Agriculture, Multan 66000, Punjab, Pakistan
[c] Tianjin Institute of Industrial Biotechnology, Chinese Academy of Sciences, Tianjin 300308, China
[d] Solar Cell Applications Research Lab, Department of Physics, Government College University Lahore, Lahore 54000, Punjab, Pakistan
[e] Core Research Facilities, King Fahd University of Petroleum & Minerals, Dhahran 31261, Saudi Arabia
[f] Departament d'Enginyeria Química, Universitat Rovira i Virgili, Av Països Catalans 26, 43007 Tarragona, Spain
[g] Chemistry Department, King Khalid Military Academy, Riyadh 11495, Saudi Arabia
[h] Chemistry Department, Faculty of Science, King Khalid University, Abha 61413, Saudi Arabia

ARTICLE INFO

Keywords:
Polyacrylic acid
Escherichia coli
Rhodamine B
Molecular docking
Nanorod

ABSTRACT

This study investigates the co-precipitation synthesis of (2 and 4 wt%) Ag and polyacrylic acid-doped SrO nanocomposites for bactericidal activities and catalytic Rhodamine B (RhB) decolorization. The objective of the investigation was to minimize the rate of electron-hole recombination of SrO to enhance charge transfer. The influence of Ag and PAA on the crystal structure, morphology, absorbance wavelength, and exciton recombination rate of SrO was studied using a systematic characterization. The binary dopants were added into SrO to reduce the crystallite size, which produces the new active sites (reduces the recombination rate) and may generate reactive oxygen species (ROS). In a neutral medium with sodium borohydride ($NaBH_4$), the synthesized nanocomposites demonstrated reasonable results for catalytic reduction of RhB dye (74.3 %). The bactericidal efficiency (96.6 %) of prepared samples was measured for Escherichia coli (*E. coli*) at various concentrations. Molecular docking studies were performed to rationale the antibacterial activity of PAA-SrO and Ag/PAA-SrO nanocomposites against $DHFR_{E.\ coli}$, $DHPS_{E.\ coli}$, and $FabI_{E.coli}$ suggested their role as inhibitors.

1. Introduction

Biological and chemical contamination of water has become a severe threat to living organisms. Agricultural, domestic, and most industrial fields produce effluents containing toxic impurities. Water contamination causes several problems as health diseases like cancer, hormonal disruption, and nervous system disorder [1]. The primary anthropogenic sources of contamination are organic dyes, pesticides, and domestic and industrial wastes. Bacterial pollution is also considered a massive ratio of general health concerns. Dye-contaminated water is released into the environment, causing eutrophication and non-esthetic pollution, producing dangerous byproducts [2]. Rhodamine B (RhB) is widely used as a tracer fluorescent as a nitrogenous cationic dye in textiles and foodstuffs. It produces cancer-causing aromatic amines through reductive anaerobic deprivation. RhB irritates the eyes, skin, and respiratory tract [3]. Using water sediment filters (fibers and ceramics), distillation and roller filters, reverse osmosis, filtered water, ozone exchange softener, water ion exchange, catalysis, and photocatalysis are some standard techniques to purify water contamination [4,5]. Besides other methods, catalysis is cost-effective and energy-efficient [6]. In catalysis and antimicrobials, metal oxides have a vast range of applications [7].

Metal oxide nanostructures (MO NSs) are attracting scrupulous attention for having remarkable properties in thermal, optical, and mechanical domains [8]. MO NSs such as Al_2O_3, MgO, CuO, TiO_2, and CaO are widely utilized for their unusual catalytic and antibacterial activity [9–13]. Furthermore, these NSs are highly notable for having

* Corresponding authors.
E-mail addresses: imran@mail.ipc.ac.cn (M. Imran), anwar@kfupm.edu.pk (A. Ul-Hamid), walid.nabgan@urv.cat (W. Nabgan), dr.muhammadikram@gcu.edu.pk (M. Ikram).

https://doi.org/10.1016/j.jphotochem.2023.114970
Received 19 April 2023; Received in revised form 18 June 2023; Accepted 19 June 2023
Available online 22 June 2023

unique physicochemical properties and high stability [12]. An attractive antibacterial agent having individual catalytic activities (cost durability, chemical stability) is titanium dioxide (TiO_2), especially the anatase phase. But the Vivo and cytotoxic experiments show that for the respiratory system, it is very harmful [14]. The SrO NSs are non-toxic, superimposed with size, good optical assets, and admirable high thermal constancy [8]. SrO, an insulating oxide with a cubic structure, represents a non-magnetic character used for medicinal purposes as a substitute for body parts. Despite being less reactive and thermally stable, SrO has gained remarkable attention in the catalytic reduction of organic impurities and antibacterial applications because of its larger surface area. For the improved CA of the catalyst, various polymer and MOs nanocrystals have been designed [15]. Small amounts of polymers, such as polyacrylic acid (PAA), enhance the surface area [16]. With SrO, intrinsic oxygen vacancies are produced, which increases charge transfer and hence improves electrochemical performance [17]. The effectiveness of SrO in degrading organic material can be enhanced by polymers such as PAA, PVP, chitosan, starch, etc. [18]. PAA possesses substantial reduction properties and decreases the rate of recombination of SrO. Ag NSs are the best choice due to their remarkable properties, such as antimicrobial activity, broad-spectrum, catalytic activity, and non-linear optical behavior.

Catalytic reduction is a process in which the chemical properties of dye molecules change by forming new chemical bonds with the addition of electrons and H-atom. The reduction of dye can change the color by breaking down the chromophore, part of the molecule that offers the dye color. Comparatively, dye degradation is fragmenting the dye molecule into smaller pieces may be caused by light, temperature, or other environmental factors. Consequently, the reduction and degradation of dye can result in decolorization chemical reactions. Reduction adds electrons to a dye molecule, while degradation breaks the dye molecule into smaller fragments [19].

Regarding bacterial pollution, Gram (-) *(Escherichia coli (E. Coli))* has a more negative charge than Gram (+) bacteria *(staphylococcus aureus (S. aureus))* [20]. So, Gram-negative bacteria possess stronger electrostatic interaction strains. The particle size to surface area ratio (smaller particle size to larger surface area) determines the efficiency of MOs NSs in inhibiting bacterial growth. The charge difference between SrO nanocomposites and bacterial membranes leads to electrostatic attraction. SrO NSs accumulated on the cell membrane surface and entered the bacteria resulting in their growth obstruction [21].

The current research aims to investigate the antimicrobial and degrading potential of Ag/PAA-doped SrO nanocomposites. Moreover, various characterization techniques (XRD, FTIR, SAED, UV, TEM, EDS, and mapping analysis) were employed to investigate the optical, morphological, and electrical properties. Further molecular docking predictions were implemented against $DHFR_{E.\ coli}$, $DHPS_{E.\ coli}$, and $FabI_{E.\ coli}$ enzyme.

2. Experimental part

2.1. Materials

Strontium chloride hexahydrate ($SrCl_2{\cdot}6H_2O$-99%), polyacrylic acid (PAA), sodium hydroxide (NaOH-98%), silver nitrate ($AgNO_3$-99.8%), and ethanol (C_2H_5OH) were procured from Sigma Aldrich (Germany).

2.2. Synthesis of SrO

0.5 M of $SrCl_2{\cdot}6H_2O$ was used to synthesize a heterogenous control sample SrO by chemical co-precipitation method under constant heating (80 °C) and stirring for 2 h. The precipitating agent (NaOH) was gradually added to the stirred solution to maintain a pH of ~ 12. Precipitates were centrifuged twice with deionized (DI) water and ethanol at 7000 rpm for 7 min and heated at 120 °C overnight, grind to obtain a fine powder. Similarly, the adequate amount of PAA (3 wt%) and Ag (2 and 4 wt%) doped SrO nanocomposites were synthesized following the same procedure shown in Fig. 1.

2.3. Catalytic activity (CA)

The CA of prepared nanocomposites was investigated in the existence of $NaBH_4$ to degrade RhB dye. Firstly, 0.1 M of the reducing agent $NaBH_4$ in DI water was integrated, and 400 µL was added to 3 mL of RhB dye solution in the dark, followed by 400 µL of SrO and (2 and 4 wt. %) Ag/PAA doped SrO. The performance of the catalytic dye degradations was investigated through UV–Vis spectroscopy to measure the decolorization percentage. The dye decolorization process occurred when the pink color dye turned colorless. The performance was assessed in acidic, basic, and neutral, whereas NaOH and H_2SO_4 were used to maintain the pH of the dye degradation solution. Calculate the % of degradation of RhB dye formula;

$$\%\ \text{Degradation} = C_o\text{-}Ct/C_o \times 100$$

where C_o = the initial absorbance, C_t = a particular time absorbance. C_o and C_t were obtained from the λ_{max} value of the absorption spectrum, measured with a UV–Vis spectrometer.

2.4. Identification and separation of E. coli bacteria

2.4.1. Isolation of E. coli

In Pakistan, Punjab province, nursing cows' mastitis milk was collected in sterilized glassware, and these cows were offered at various marketplaces, veterinary farms, and clinics. On 5% sheep blood agar, collected samples were cultured, preserved at 36 °C for 24 h, and then applied on the surface of MacConkey-agar (MA) to segregate *E. coli* bacteria. Biochemical essays, like catalase and coagulase, morphological evaluation, and Gram staining, characterized the isolated colonies.

2.4.2. Identification and characterization of bacterial isolates

The preparation of *E. coli* was determined using colony morphology with the Gram stain and numerous biochemical tests with Bergey's Handbook of Determinative Microbiology.

2.4.2.1. Antibiotic susceptibility. Bauer et al. [22] disk diffusion method was accomplished on Mueller Hinton agar (MHA) for the antibiotic susceptibility test. For the bactericidal activity, used Ciprofloxacin (Cip) 5 µg was used to test *E. coli* antibiotic resistance [23]. To achieve a turbidness of 0.50, a pure *E. coli* culture was obtained according to the MacFarland standard. The plates were stored at 36 °C for 24 h before being examined following Clinical and Laboratory Standard Institute guidelines [24].

2.4.3. Bactericidal activity

The antimicrobial efficacy of SrO and (2 and 4 wt%) Ag/PAA-SrO nanocomposites were evaluated against *E. coli* through agar well diffusion method through inhibition zones. MA Petri dishes were incubated with *E. coli* bacteria at a concentration of 1.5×10^8 CFU/mL, and the plates were then placed in the incubator. The holes in the agar plates, which were 6 mm in diameter, were created with a sterile cork borer. The wells were loaded with varying concentrations of SrO and doped SrO nanocomposites, ranging (0.5 mg/50 µL) to (1.0 mg/50 µL). DI water (50 µL) was used as a -ve control, whereas ciprofloxacin (0.005 mg/50 µL) was used as a + ve control.

2.5. Molecular docking studies

Various nanoparticles and nanocomposite systems have been found as good antimicrobial agents. Although nanocomposites biological potential is well-documented, the exact mechanism behind their biological processes must be explored. Computational methods, particularly

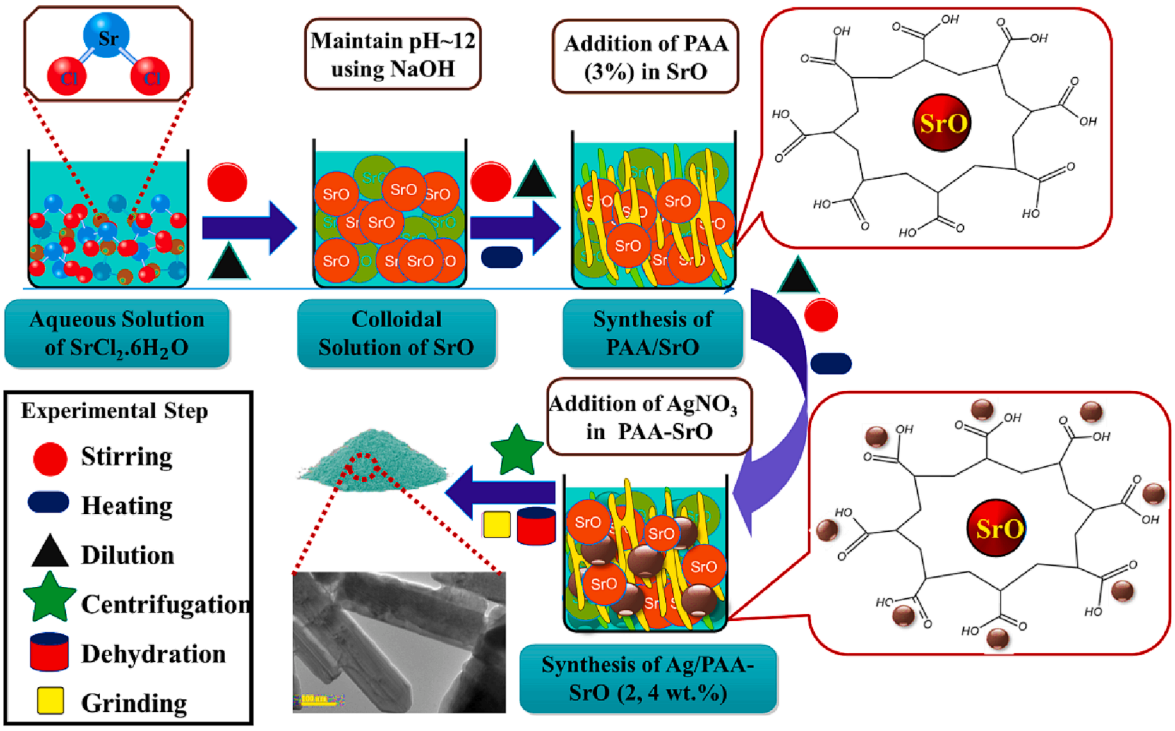

Fig. 1. Synthesis of Ag/PAA-doped SrO nanocomposites.

molecular docking investigation, enabled scientists around the globe to have an in-depth analysis of various interactions and mechanisms. Considering the good antibacterial activity of synthesized nanocomposites here, we performed their molecular docking studies against selected enzymes as possible targets for inhibition. Three enzymes i.e., dihydrofolate reductase ($DHFR_{E.\ coli}$), dihydropteroate synthase ($DHPS_{E.\ coli}$), and Enoyl-[acyl-carrier-protein] (ACP) reductase ($FabI_{E.coli}$) were selected [25–28], and their 3D-structural coordinates were retrieved from the protein data bank. The accession codes used for $DHFR_{E.\ coli}$, $DHPS_{E.\ coli}$, and $FabI_{E.coli}$ were 2ANO [29], 5U0W [30], and 1MFP [28], respectively.

ICM Molsoft v3.8-7d (Molsoft L.L.C., La Jolla, CA) predicted molecular docking [31]. The preparation of protein structures involved the addition of polar H-atoms and gastegier charges, removal of water molecules and native ligands, and energy minimization. Later, the docking site was determined by specifying 10 Å near the native ligand in each case. Interaction patterns analysis of docked complexes and graphical representation was done using ICM viewer and Pymol software, while ligand structures were built using the LigEdit tool of ICM.

3. Results and discussion

For the preparation of Ag/PAA-doped SrO nanocomposites, the fixed amount of PAA (3 wt%) and Ag (2 and 4 wt%) were added into SrO nanocomposites through the co-precipitation method (Fig. 1).

The crystallographic plane structure and phase purity of SrO and Ag/PAA-SrO were investigated through XRD in 2θ ranges from 10 to 80° (Fig. 2a). XRD pattern shows well-defined diffracted peaks angle at 25.35°, 32.56°, and 49.9° for the planes (1 1 0), (0 0 1), and (2 2 0), respectively. These planes are well matched with the cubic phase of SrO, along the space group Fm3m confirmed by (JCPDS card 00–006-0520). Additionally, the other diffraction peaks at 36.01° and 75.5° ascribed to (1 1 2) and (2 2 0) planes of tetragonal SrO_2 (with JCPDS card 00–006-0520, space group I4/mmm). Furthermore, the diffraction peaks observed at 43.5°, 46.6°, 54.42°, 57.38°, and 65.61° correspond to planes (2 0 0), (4 0 0), (5 1 1), (2 1 0), and (3 2 2) of orthorhombic $Sr(OH)_2$ with standard spectrum (JCPDS card 01-071-2365) of synthesized material [32]. Crystallinity was reduced upon the incorporation of PAA, attributed to the amorphous behavior of the polymer. The two distinct peaks were observed upon Ag doping at 20.25° and 25.23° for (2 1 0) and (1 1 0) planes of orthorhombic Ag crystal structure (JCPDS No: 96-150-9552). According to the Debye Scherrer formula ($D = 0.89\,\lambda/\beta\cos\theta$), the average crystallite size of the SrO, PAA-SrO, and Ag/PAA doped SrO (2 and 4 wt.%) was ~38.60, 36.80, 35.46 and 31.78 nm respectively previous reported [33].

To verify the purity of the sample and examine the chemical structure, Ag/PAA-SrO nanocomposites were characterized by FTIR spectra (Fig. 2b). The broad transmittance bands that emerge at 3366 cm^{-1} originate from the vibrational stretching modes of the OH bond of H_2O [34]. The band at 1652 cm^{-1} manifested to hydroxyl group vibrational bending mode (O–H) [35]. The 1494 and 602 cm^{-1} bands correspond to asymmetric stretching vibration and out-of-plane bending vibration of Sr–O, confirming the successful formation of SrO nanocomposites [32,36]. Upon Ag/PAA incorporation, results show no shift in the transmittance spectra. In addition, the SAED pattern of SrO and Ag/PAA-SrO nanocomposites showed bright rings associated with distinct XRD facets (0 0 1), (1 1 2), (1 1 0), and (0 0 2) (Fig. 2c-f).

For the optical evaluation of synthesized Ag/PAA-doped SrO nanocomposites, UV–Vis spectra were examined from 200 to 500 nm (Fig. 3a). The observed spectra indicated the absorption band at 242 nm for SrO [37]. The band gap energy (E_g) was calculated at 3.86 eV for SrO. As Ag and PAA were added, a decrease in E_g was attributed to a bathochromic shift representing a change in crystallite size for PAA-SrO [8]. The Tauc plot equation calculated the E_g of SrO and Ag/PAA-doped SrO nanocomposites to be 3.86, 3.75, 3.63, and 3.49 eV, respectively (Fig. 3b) [37]. The (n–π*) transition band has dramatically decreased the E_g from 3.86 to 3.49 eV. This E_g reduction may make electron transport in nanocomposites easier, improving CA.

TEM micrographs investigate the morphology of SrO and Ag/PAA doped SrO nanocomposites (Fig. 4a-d). As reported in Fig. 4a, nanorods of SrO were arranged in a bushlike assembly with a nonuniform diameter. Incorporating PAA into SrO causes the formation of agglomerated, distinctive nanorod-like structures that could enhance charge carrier mobility throughout the catalytic process. The catalytic activity of SrO

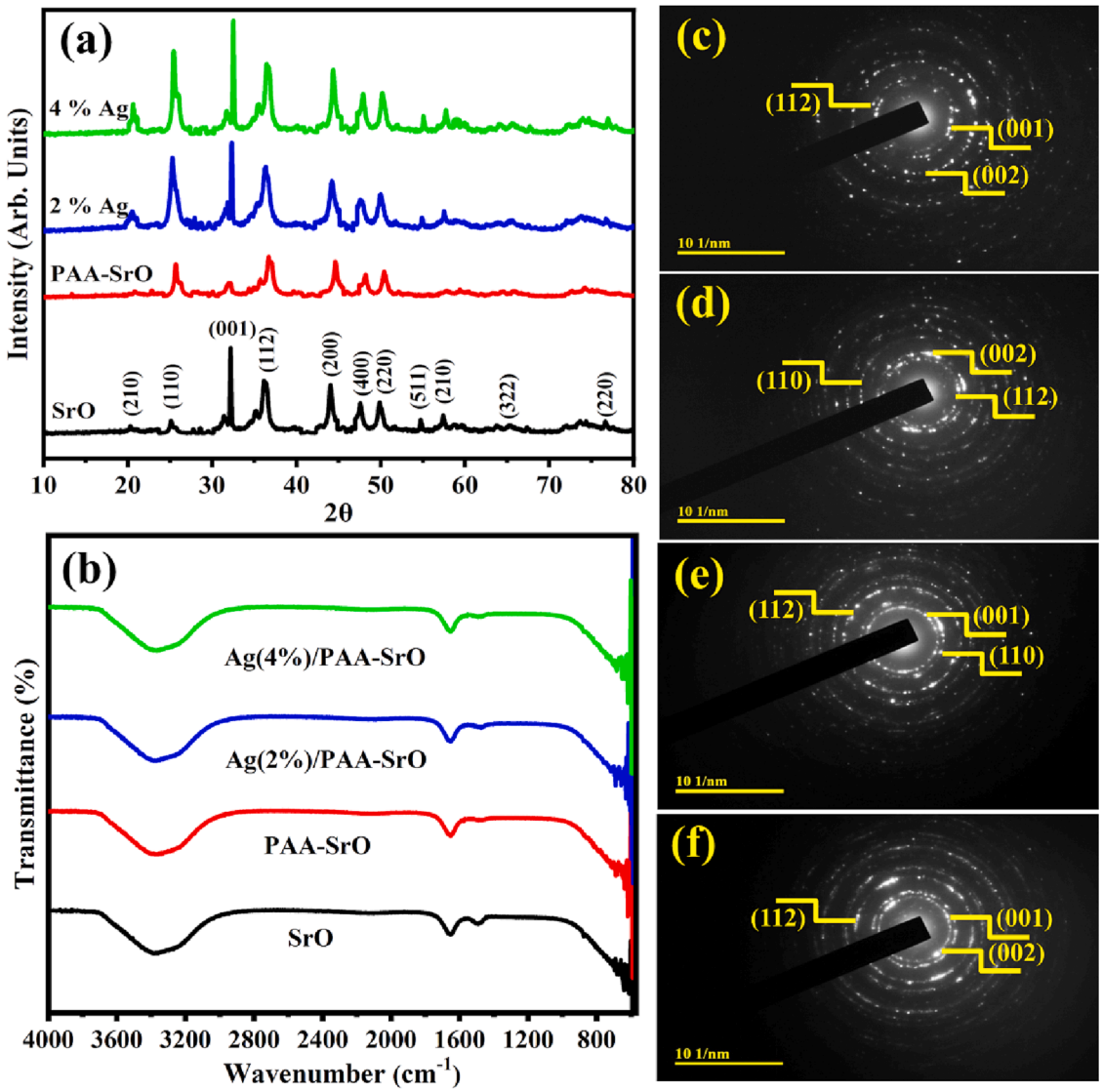

Fig. 2. (a) XRD pattern, (b) FTIR spectra, (c–f) SAED images of SrO, PAA-SrO, and Ag/PAA-SrO (2 and 4 wt%) nanocomposites.

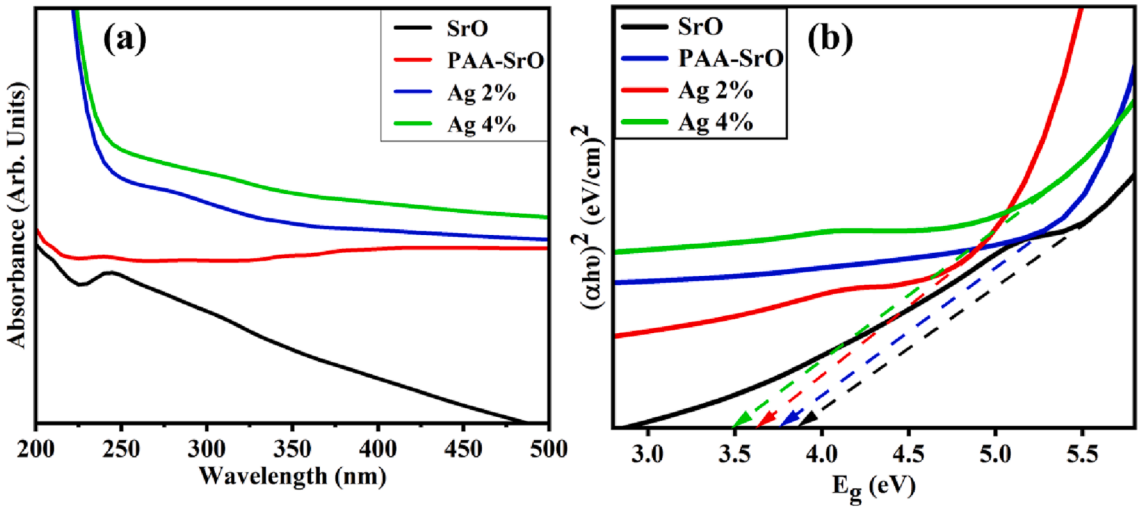

Fig. 3. (a) UV–vis spectra (b) band gap UV–vis spectra of SrO, PAA-SrO and Ag/PAA-SrO (2 and 4 wt%) nanocomposites.

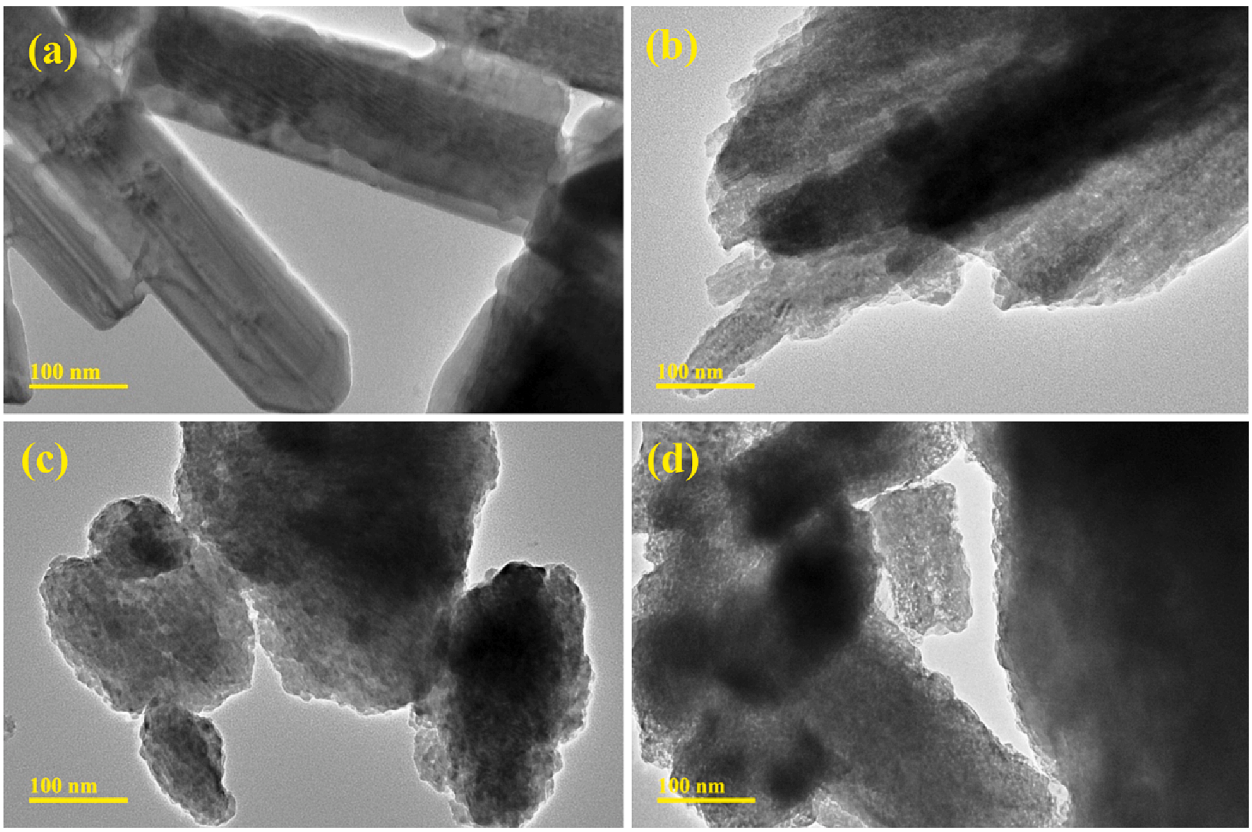

Fig. 4. TEM micrograph of (a) SrO, (b) PAA-SrO, and (c-d) Ag/PAA doped SrO (2 and 4 wt%) nanocomposites.

will increase due to the high surface area provided by the aggregated nanorods [38]. The addition of 2 wt% of Ag to the binary system PAA-SrO produced high aggregation and chunk-like morphology. Agglomeration increased with increasing Ag concentration, resulting in a considerable nanorod-type structure.

HR-TEM microscopy was used to calculate d-spacing in SrO, and Ag/PAA doped SrO nanocomposites, as shown in Fig. S1a-d. The measured d-spacing values of host and doped SrO nanocomposites were 0.295, 0.293, 0.278, and 0.267 nm, well organized with XRD results.

The elemental identification of undoped and doped SrO nanocomposites was confirmed using EDS analysis (Fig. S2a-d). The presence of SrO is confirmed by strontium (Sr) and oxygen (O) peaks. Silver (Ag) and carbon (C) peaks in EDS spectra of Ag/PAA-SrO NSs indicate the successful addition of dopants into the SrO. In addition, a chlorine (Cl) peak was detected, which was linked directly to the precursors used in the synthesis. The incorporations of NaOH during the synthesis of pH maintenance were attributed to the sodium (Na) peaks. The atomic distribution of Ag/PAA doped SrO nanocomposites was determined by mapping results revealing that six elements (Sr, O, Ag, C, Na, and Cl) were uniformly dispersed with various elemental concentrations via different colors (Fig. S2e).

The redox reaction occurred in the catalysis mechanism; RhB is oxidizing species, while $NaBH_4$ acts as electron donating species. In the presence of $NaBH_4$, decolorization of RhB occurred, which was a sluggish reaction. The activation energy was reduced when pure and doped SrO was combined with RhB, which increased the reaction rate. The electron relay system facilitated by the SrO and Ag/PAA doped SrO makes it easier for electrons to be transported from the receiver to the RhB dye. Due to their small crystallite size, nanocatalysts offer an advantageously high surface-to-volume ratio for dye degradation. An XRD investigation found that crystallite size reduces as Ag concentration increases to optimal levels; this increases the active sites, ensure in a significant CA for the decolorization of RhB dye. The electron was absorbed on the surface of RhB, which was then transformed into LRhB (Fig. S3).

According to the findings of the experiments, the most effective dye degradation occurred in a neutral medium, as shown in Fig. 5. $NaBH_4$ serves as an electron relay, transferring electrons and limiting CA in the absence of a nanocatalyst. The prepared nanocatalyst (400 μL) has been added to the dye-prepared solution, improving dye degradation and catalytic performance to 74.3 % dye in 10 min in a neutral medium. It is important to note that the % of dye degradation is directly related to the pH value of the medium. Large decolorization of RhB occurred in a neutral medium which are 74.3, 71.2, 72 and 73.7 %; in an acidic medium 65.1, 65.8, 67.1, and 67.3 %, and basic medium, 53.0, 51.5, 60.7 and 51.5 % for SrO, PAA-SrO and (2, 4 wt%) Ag/PAA doepd SrO in 10 min (Fig. 5a-c).

The textile industry is one of the most chemically intensive industries, and its real wastewater includes dangerous dyes, pigments, suspended or dissolved solids, and heavy metals. The real wastewater was collected from a local textile industry in Lahore, Pakistan; after collection, the real wastewater was stored at 37 °C. Using a UV–vis spectrophotometer, decolorizing real wastewater is an essential parameter for demonstrating the treatment performance of effluent. CA of prepared nanocomposites was investigated in the presence of $NaBH_4$ to degrade the real wastewater. Pure and (2 and 4 wt%) Ag/PAA doped SrO expressed the degradation of industrial wastewater (pH = 8.77) 43, 44.2, 63, and 69.47 %, respectively in 10 min (Fig. 5d). The degradation efficiency of synthesized nanocomposites for RhB dye synchronized with real wastewater results.

Despite lacking H^+ ions in the basic medium, NaOH excess OH^- ions stick to the nanocatalyst surface, creating a -ve charge on the prepared material used as a catalyst. Adsorption occurs when the negative surface charge of the nanocatalyst is attracted to the positive surface charge of the cationic RhB dyes in the natural medium. Increased adsorption in a basic medium promotes considerable contact between the positive and

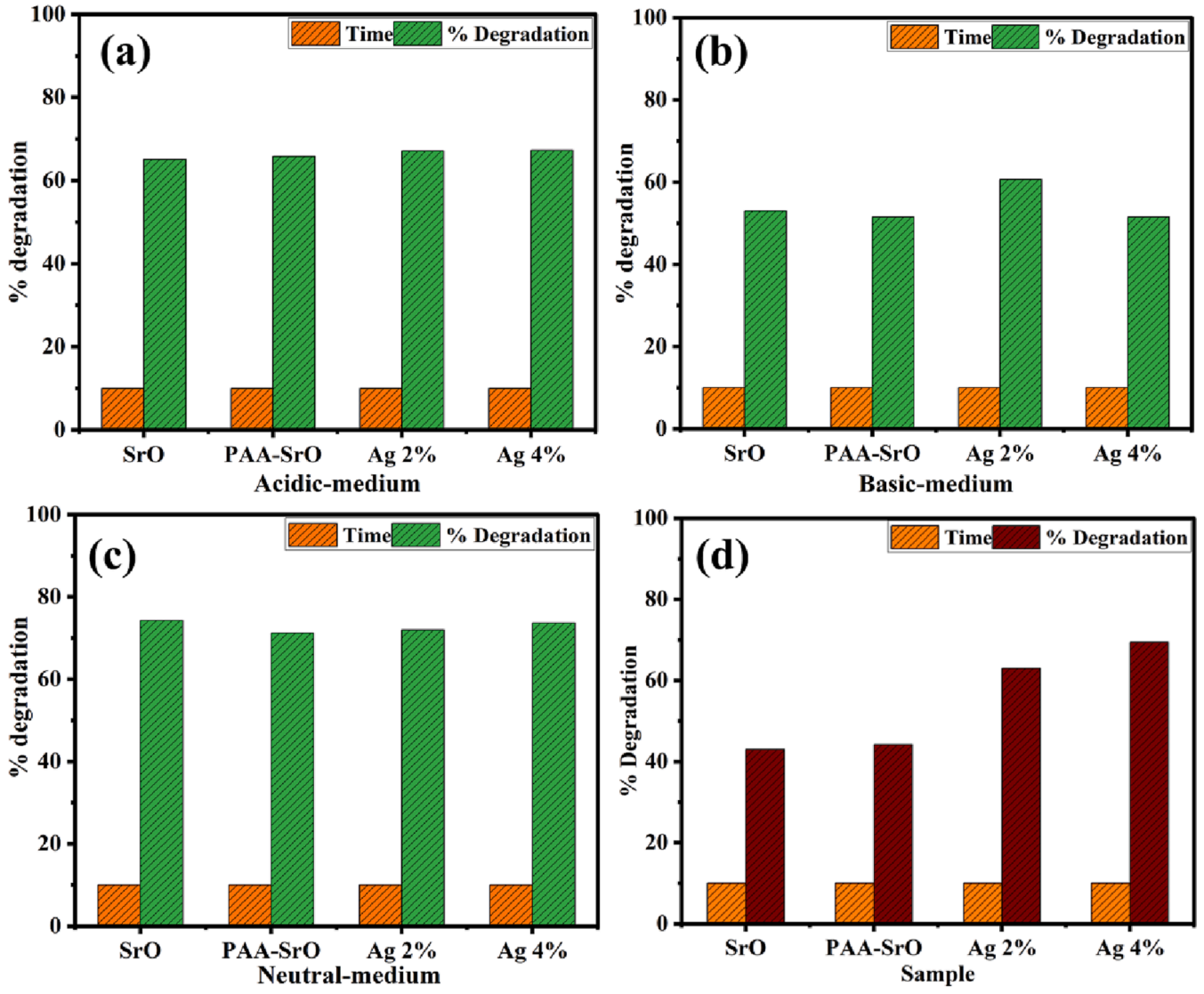

Fig. 5. Catalytic activity of SrO and doped SrO nanocomposites in (a) acidic, (b) basic and (c) neutral media (d) real wastewater degradation in 10 min.

negative charged surfaces of RhB and the nanocatalyst, leading to high dye degradation efficiency [39].

$NaBH_4$ transfers e^-/h^+ to the surface of nanocomposites and forms metal-hydrogen covalent linkages. RhB dye adsorbs onto the active site leading to dye degradation by capturing e^- and adsorbed H. In nanostructures, adsorption of the dye molecules and BH_4^- ion is enhanced; having several active sites leads them to react [40]. Leuco-Rhodamine B (LRhB; a reduced form of RhB) desorbs from the active site directing to the re-emergence of the catalyst for its further CA. During CA, a redox reaction occurs, which involves the transfer of electrons (Fig. S3). Absenteeism of nanocomposites, the catalytic activity reaction is protracted. As the activation energy decreases, the addition of nanocomposites leads to an increase in the reaction rate.

Increased CA was observed for Ag/PAA-doped SrO nanocomposites due to their high surface area. Consequently, the catalytic reduction of RhB by Ag/PAA (4 wt%) doped SrO nanocomposites is considerably enhanced, and the dye is degraded effectively (Fig. S4a). The rate constants (k) for catalytic reduction kinetics have been calculated by quantifying the slopes of $\ln(C_o/C_t)$ against time. The degradation rate constant k was calculated to be 0.12397 ± 0.0204, 0.12198 ± 0.02197, 0.125583 ± 0.02358, and 0.12465 ± 0.02591 min^{-1} for undoped and doped SrO, respectively (Fig. S4b).

The inhibition zone of SrO, PAA-SrO, and (2 and 4 wt%) Ag-doped PAA SrO nanocomposites for G -ve bacteria were calculated through the agar well diffusion method in Table 1. At various concentrations, the inhibition zoon of SrO and doped SrO nanocomposites was examined against *E. coli* bacteria. The low and high concentrations zones of inhibition were measured as 1.65–3.85 and 2.205–4.60 mm, respectively. Ciprofloxacin was used as a positive control, and its inhibition zones against the low and high concentrations (4.95 mm) were significantly larger than those of DI water (0 mm) (Fig. S5a-b). The percentage of efficacy against *E. coli* increases from (33 to 77 %) at low concentrations and from (41 to 92 %) at high concentrations accordingly (Fig. S5b). In

Table 1
Bactericidal activity of SrO, PAA-SrO, and (2 and 4 wt%) Ag doped PAA-SrO.

Samples	*E. coli*	
	Inhibition zone (mm)	
	0.5 mg/50 μL	1.0 mg/50 μL
SrO	1.65	2.05
PAA-SrO	2.25	2.55
Ag/PAA-SrO (2%)	3.05	3.55
Ag/PAA- SrO (4%)	3.85	4.60
Ciprofloxacin	4.95	4.95
DI water	0	0

conclusion, the results reveal that the Ag/PAA doped SrO nanocomposites exceeded the antibacterial efficiency of the G -ve bacterial strain.

With the addition of PAA, inhibitory zones increased due to carboxylic and hydroxyl groups, which boosted the formation of ROS. It is conceivable that ROS made it easier for metal ions to discharge, which ultimately led to the death of bacterial cells. Additionally, Ag doping had a more effective bactericidal effect because Ag negatively influences metal oxide particle formation, resulting in smaller particle sizes and increased contact with SrO nanocomposites and bacterial cells. According to the findings, Ag/PAA doped-SrO nanocomposites possessed a more robust bactericidal activity against *E. coli*, a type of Gram-negative bacteria distinguished by its thicker cell walls and more complicated structures. The prepared nanomaterials' crystallite size, nanostructure, and active sites influence oxidative stress tolerance. The Ag/PAA was added into SrO to reduce the crystallite size, which produces the new active sites and may generate ROS to enhance the antimicrobial activity [41,42].

The chemical process generates ROS like superoxide anion radical ($^*O^{-2}$), hydroxyl radical (*OH), and hydrogen peroxide radicals ($^*H_2O_2$). As a result of the interaction between electrostatic forces and hydrophobic, certain transition metal oxides possess antimicrobial activity. As shown in Fig. S6, Sr^{2+} destroys bacterial membrane stability to increase the antibacterial activity. The strontium cation (Sr^{2+}) interlinked with bacterial cell walls causes microbial collapse, DNA damage, and pathogenic cross-linkage disruption [43,44].

Molecular docking analysis of prepared undoped and doped SrO nanocomposites were performed for in-depth analysis of interactions responsible for their bactericidal activity and to explore their role as possible inhibitors of selected enzyme target $DHFR_{E.\ coli}$, $DHPS_{E.\ coli}$, and $FabI_{E.coli}$ in the current study. In the case of $DHFR_{E.\ coli}$, both PAA-SrO and Ag/PAA-SrO nanoparticles revealed moderate binding tendency inside active pocket having binding scores −4.761 and −7.552 kcal/mol, respectively. Where PAA-SrO interacted through H-bond (1.6 Å) with Ala7 and pi-alkyl interaction with Tyr100 while Ag/PAA-SrO showed two H-bond relations i.e. Asp27 (2.8 and 3.0 Å) alongside Pi-alkyl interaction with Tyr100 as depicted in Fig. 6. These docked complexes were also compared with known Antibiotic ciprofloxacin-$DHFR_{E.\ coli}$ complex (binding score: −9.978 kcal/mol).

The docking tendency of synthesized nanocomposites was also evaluated against DHPS*E. coli*, another essential enzyme of the folate biosynthetic pathway. The docked complexes for PAA-SrO and Ag/PAA-SrO NPs revealed much better binding scores (-8.493 and −8.881 kcal/mol) and interactions with active site residues. Four H-bonds were observed in the case of the PAA-SrO complex i.e., Arg255 (1.7 and 2.7 Å), Ile20 (2.7 Å), and Asn22 (1.9 Å), while Ag/PAA-SrO NPs showed involvement of three H-bonds as Asp56 (2.3 Å), Asp96 (2.7 Å) and Arg255 (1.8 Å) shown in Fig. 7. The binding score observed in case of ciprofloxacin-DHPS*E. coli* complex was −9.119 kcal/mol.

Similarly, docking complexes were generated and analyzed inside the active pocket of FabI (a well-known target for antibiotics). The best-docked complex obtained in the case of PAA-SrO showed a binding score of −7.683 kcal/mol having H-bonds with Ser19 (1.9 Å), Ile20 (1.6 Å) and Thr194 (1.7 Å) while Ag/PAA-SrO NPs revealed H-bonds with Gly13 (2.9 Å), Ser19 (2.4 Å), Ile20 (2.1 Å) and Ile92 (2.3 Å) having binding score −10.583 kcal/mol as depicted in Fig. S7. Ciprofloxacin docked complex with $FabI_{E.coli}$ revealed a binding score of −11.037 kcal/mol. These nanocomposites may be inhibitors of $DHFR_{E.\ coli}$, $DHPS_{E.\ coli}$, and $FabI_{E.coli}$, as suggested by molecular docking. This opened new horizons for the use of nanoparticles as new Antibiotic agents.

4. Conclusion

This current research aimed to synthesize SrO and Ag/PAA-doped SrO nanocomposites through co-precipitation and improve their bactericidal and catalytic properties. The XRD analysis demonstrated that SrO has a cubic structure, and crystallite size ranges between 38.60 and 31.78 nm upon adding Ag and PAA. FTIR analysis was utilized to categorize the out-of-plane bending vibration of Sr-O. The SAED pattern revealed that the synthesized nanocomposites were crystalline and analogous to the XRD results. The bathochromic or red shift in electronic

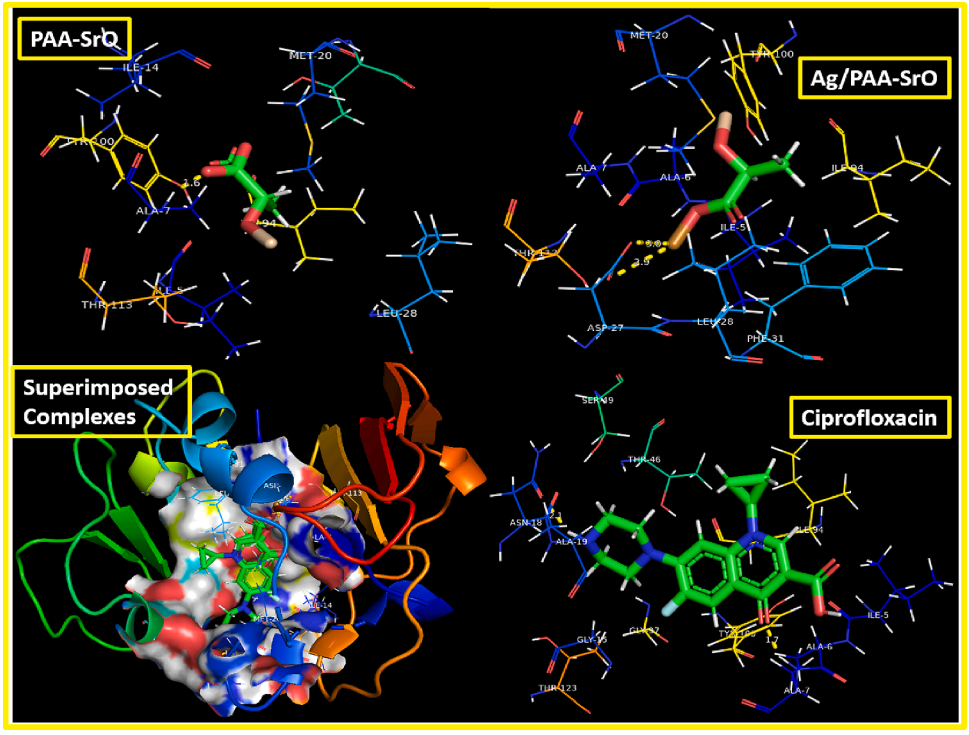

Fig. 6. Binding interaction pattern of PAA-SrO, Ag/PAA-SrO nanocomposites, and ciprofloxacin inside active pocket of $DHFR_{E.\ coli}$.

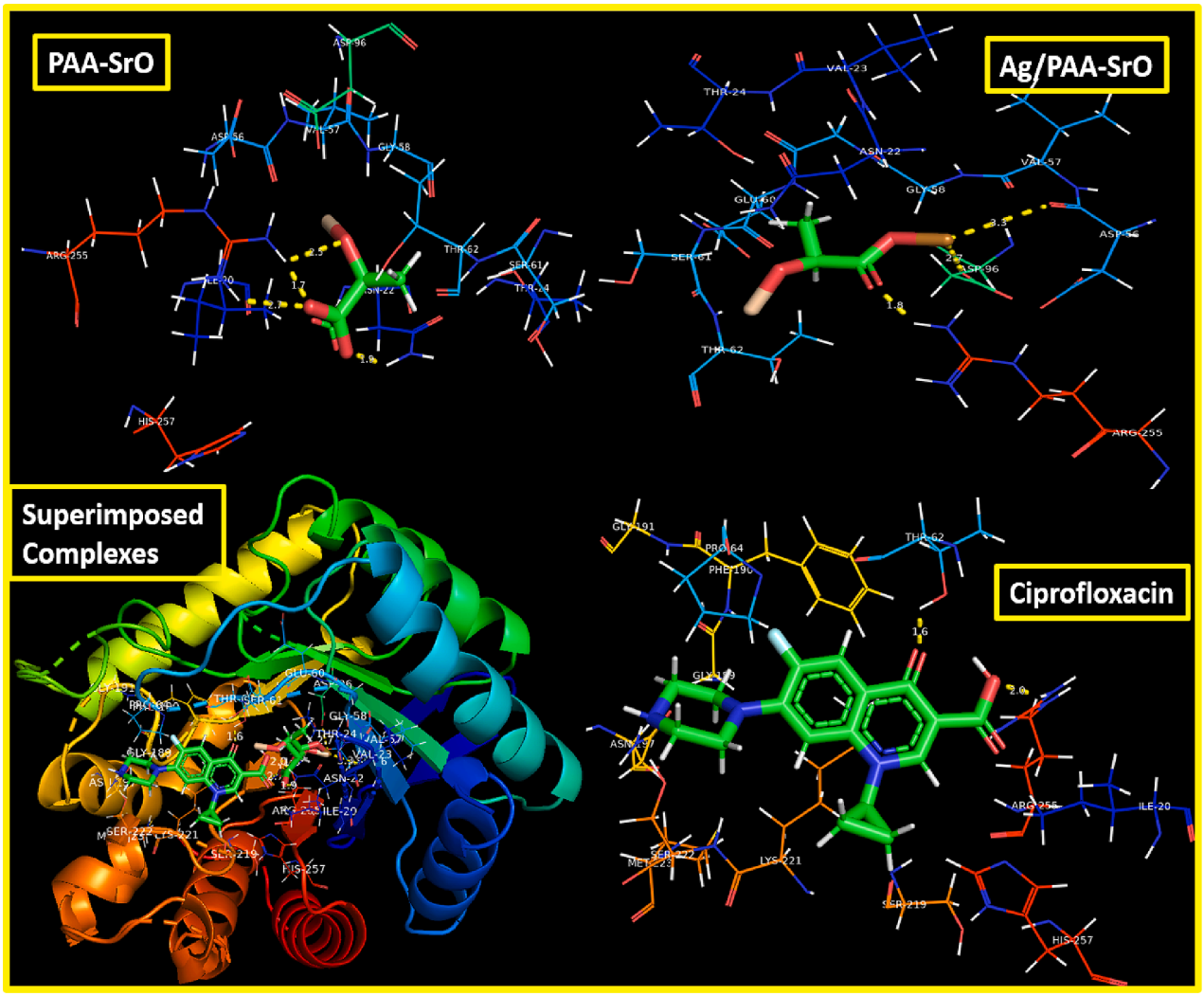

Fig. 7. Binding interaction pattern of PAA-SrO and Ag/PAA-SrO nanocomposites and ciprofloxacin inside active pocket of $DHPS_{E.\ coli}$.

spectra caused by incorporating Ag and PAA resulted in a decrease in band gap energy. The morphological analysis confirmed the emergence of a nanorod-like structure of SrO, and the agglomeration was increased upon incorporating Ag/PAA. The EDS examination of nanocomposites provided conclusive evidence that Sr, O, and Ag samples. The synthesized nanocomposites degraded RhB dye in acidic, basic, neutral conditions and real wastewater was 67.3 %, 60.7 %, 74.3 %, and 69.47 % respectively. The synthesized Ag/PAA doped SrO nanocomposites manifested inhibition zone at various concentrations (3.85 and 4.60 mm, respectively) against *E-coli* bacteria, compared to ciprofloxacin. *In silico* studies predicted the synthesized nanocomposites PAA-SrO and Ag/PAA-SrO as possible inhibitors of $DHFR_{E.\ coli}$, $DHPS_{E.\ coli}$, and $FabI_{E.\ coli}$. In conclusion, SrO nanocomposite with Ag/PAA dopant concentration is an effective inhibitor against *E. coli* bacteria and a catalyst for decolorizing RhB.

CRediT authorship contribution statement

Husnain Shahzad: Writing – original draft, Formal analysis. **Muhammad Imran:** Writing – original draft, Supervision, Funding acquisition. **Ali Haider:** Resources, Conceptualization. **Sadia Naz:** Writing – review & editing, Investigation, Conceptualization. **Ehtisham Umar:** Resources, Data curation. **Anwar Ul-Hamid:** Methodology, Formal analysis. **Walid Nabgan:** Funding acquisition, Formal analysis, Conceptualization. **Mohammed M. Algaradah:** Writing – review & editing, Funding acquisition, Conceptualization. **Ahmed M. Fouda:** Writing – review & editing, Methodology, Funding acquisition. **Junaid Haider:** Writing – review & editing, Data curation. **Muhammad Ikram:** Writing – original draft, Supervision, Funding acquisition.

Declaration of Competing Interest

The authors declare that they have no known competing financial interests or personal relationships that could have appeared to influence the work reported in this paper.

Data availability

Data will be made available on request.

Acknowledgment

Authors are thankful to HEC, Pakistan, through NRPU-20-17615 and express gratitude for the support received from Universitat Rovira i Virgili under the Maria Zambrano Programme (Reference number: 2021URV-MZ-10). The authors extend their appreciation to the Deanship of Scientific Research at King Khalid University, Saudi Arabia for funding this work through Small Groups Project under Grant Number (RGP.1/248/44).

Data availability statement

On demand.

Appendix A. Supplementary data

Supplementary data to this article can be found online at https://doi.org/10.1016/j.jphotochem.2023.114970.

References

[1] J. Li, P. Jin, W. Dai, C. Wang, R. Li, T. Wu, C. Tang, Excellent performance for water purification achieved by activated porous boron nitride nanosheets, Mater. Chem. Phys. 196 (2017) 186–193.

[2] M. Panizza, G. Cerisola, Direct And Mediated Anodic Oxidation of Organic Pollutants, Chem. Rev. 109 (12) (2009) 6541–6569.

[3] S.S. Thind, G. Wu, A. Chen, Synthesis of mesoporous nitrogen–tungsten co-doped TiO2 photocatalysts with high visible light activity, Appl. Catal. B Environ. 111–112 (2012) 38–45.

[4] S. Sharma, A. Bhattacharya, Drinking water contamination and treatment techniques, Appl. Water. Sci. 7 (3) (2017) 1043–1067.

[5] D. Cambié, C. Bottecchia, N.J.W. Straathof, V. Hessel, T. Noël, Applications of Continuous-Flow Photochemistry in Organic Synthesis, Mater. Sci. Water Treat. Chem. Rev. 116 (17) (2016) 10276–10341.

[6] M. Junaid, M. Imran, M. Ikram, M. Naz, M. Aqeel, H. Afzal, H. Majeed, S. Ali, The study of Fe-doped CdS nanoparticle-assisted photocatalytic degradation of organic dye in wastewater, Appl. Nanosci. 9 (8) (2019) 1593–1602.

[7] R. Gusain, K. Gupta, P. Joshi, O.P. Khatri, Adsorptive removal and photocatalytic degradation of organic pollutants using metal oxides and their composites: A comprehensive review, Adv. Colloid Interface Sci. 272 (2019).

[8] M. Ikram, S. Abbas, A. Haider, S. Naz, S.O.A. Ahmad, J. Haider, A. Ul-Hamid, A. Shahzadi, I. Shahzadi, A.R. Butt, Efficient dye degradation, antimicrobial behavior and molecular docking analysis of gold (Au) and cellulose nanocrystals (CNC)-doped strontium oxide nanocomposites, J. Nanostruct. Chem. 12 (5) (2022) 933–950.

[9] T. Chakraborty, A. Chakraborty, S. Maity, D. Das, T. Chattopadhyay, Conglomerated system of Ag nanoparticles decorated Al2O3 supported cobalt and copper complexes with enhanced catalytic activity for oxidation reactions, Mol. Cat. 462 (2019) 104–113.

[10] M. Nasrollahzadeh, Z. Issaabadi, S.M. Sajadi, Green synthesis of a Cu/MgO nanocomposite by Cassytha filiformis L. extract and investigation of its catalytic activity in the reduction of methylene blue, congo red and nitro compounds in aqueous media, RSC Adv. 8 (7) (2018) 3723–3735.

[11] S. Iqbal, M. Javed, A. Bahadur, M.A. Qamar, M. Ahmad, M. Shoaib, M. Raheel, N. Ahmad, M.B. Akbar, H. Li, Controlled synthesis of Ag-doped CuO nanoparticles as a core with poly(acrylic acid) microgel shell for efficient removal of methylene blue under visible light, J. Mater. Sci Mater Electron 31 (11) (2020) 8423–8435.

[12] Y. Ma, Y. Guo, S. Wu, Z. Lv, Q. Zhang, Y. Ke, Titanium dioxide nanoparticles induce size-dependent cytotoxicity and genomic DNA hypomethylation in human respiratory cells, RSC Adv. 7 (38) (2017) 23560–23572.

[13] M. Ikram, M. Saeed, J. Haider, A. Haider, A. Ul-Hamid, A. Shahzadi, W. Nabgan, A. Rafique, S. Dilpazir, S. Ali, Facile synthesis of chitosan-grafted polyacrylic acid-doped CaO nanoparticle for catalytic and antimicrobial potential, Appl. Nanosci. 12 (9) (2022) 2657–2670.

[14] P. Pichat, A Brief Survey of the Potential Health Risks of TiO2 Particles and TiO2-Containing Photocatalytic or Non-Photocatalytic Materials, 13(3) (2010) 238-246.

[15] Z.A. Hu, L.J. Ren, X.J. Feng, Y.P. Wang, Y.Y. Yang, J. Shi, L.P. Mo, Z.Q. Lei, Platinum-modified polyaniline/polysulfone composite film electrodes and their electrocatalytic activity for methanol oxidation, Electrochem. Commun. 9 (1) (2007) 97–102.

[16] H.H. Zhou, S.Q. Jiao, J.H. Chen, W.Z. Wei, Y.F. Kuang, Effects of conductive polyaniline (PANI) preparation and platinum electrodeposition on electroactivity of methanol oxidation, J Appl Electrochem 34 (4) (2004) 455–459.

[17] C.-C. Yang, T. Wu, H.-R. Chen, T.-H. Hsieh, K.-S. Ho, C.-W.J.I.J.E.S. Kuo, Platinum particles embedded into nanowires of polyaniline doped with poly (acrylic acid-co-maleic acid) as electrocatalyst for methanol oxidation, 6(5) (2011) 1642-1654.

[18] Y. Hu, X. Jiang, Y. Ding, H. Ge, Y. Yuan, C. Yang, Synthesis and characterization of chitosan–poly(acrylic acid) nanoparticles, Biomaterials 23 (15) (2002) 3193–3201.

[19] P. Bansal, G.R. Chaudhary, S.K. Mehta, Comparative study of catalytic activity of ZrO2 nanoparticles for sonocatalytic and photocatalytic degradation of cationic and anionic dyes, Chem. Eng. J. 280 (2015) 475–485.

[20] Y.-C. Chung, Y.P. Su, C.-C. Chen, G. Jia, H.L. Wang, J.G. Wu, J.G.J.A.p.s. Lin, Relationship between antibacterial activity of chitosan and surface characteristics of cell wall, 25(7) (2004) 932-936.

[21] S. Jagadeeshan, R. Parsanathan, Nano-metal Oxides for Antibacterial Activity, in: M. Naushad, S. Rajendran, F. Gracia (Eds.), Advanced Nanostructured Materials for Environmental Remediation, Springer International Publishing, Cham, 2019, pp. 59–90.

[22] G.L. Furtado, A.A. Medeiros, Single-disk diffusion testing (Kirby-Bauer) of susceptibility of Proteus mirabilis to chloramphenicol: significance of the intermediate category, 12(4) (1980) 550-553.

[23] A. Feuerstein, N. Scuda, C. Klose, A. Hoffmann, A. Melchner, K. Boll, A. Rettinger, S. Fell, R.K. Straubinger, J.M. Riehm, Antimicrobial Resistance, Serologic and Molecular Characterization of E. coli Isolated from Calves with Severe or Fatal Enteritis in Bavaria, Germany 11 (1) (2022) 23.

[24] V.M. Pierce, A.J. Mathers, Setting Antimicrobial Susceptibility Testing Breakpoints: A Primer for Pediatric Infectious Diseases Specialists on the Clinical and Laboratory Standards Institute Approach, J. Pediatric Infectious Diseases Soc. 11 (2) (2022) 73–80.

[25] M.V. Raimondi, O. Randazzo, M. La Franca, G. Barone, E. Vignoni, D. Rossi, S. Collina, D.H.F.R. Inhibitors, Reading the Past for Discovering Novel Anticancer Agents, Molecules (2019).

[26] B.I. Schweitzer, A.P. Dicker, J.R. Bertino, Dihydrofolate reductase as a therapeutic target, FASEB J. 4 (8) (1990) 2441–2452.

[27] T.L. Mistry, L. Truong, A.K. Ghosh, M.E. Johnson, S. Mehboob, Benzimidazole-Based FabI Inhibitors: A Promising Novel Scaffold for Anti-staphylococcal Drug Development, ACS Infect. Dis. 3 (1) (2017) 54–61.

[28] M.A. Seefeld, W.H. Miller, K.A. Newlander, W.J. Burgess, W.E. DeWolf, P.A. Elkins, M.S. Head, D.R. Jakas, C.A. Janson, P.M. Keller, P.J. Manley, T.D. Moore, D. J. Payne, S. Pearson, B.J. Polizzi, X. Qiu, S.F. Rittenhouse, I.N. Uzinskas, N. G. Wallis, W.F. Huffman, Indole Naphthyridinones as Inhibitors of Bacterial Enoyl-ACP Reductases FabI and FabK, J. Med. Chem. 46 (9) (2003) 1627–1635.

[29] R.L. Summerfield, D.M. Daigle, S. Mayer, D. Mallik, D.W. Hughes, S.G. Jackson, M. Sulek, M.G. Organ, E.D. Brown, M.S. Junop, A 2.13 Å Structure of E. coli Dihydrofolate Reductase Bound to a Novel Competitive Inhibitor Reveals a New Binding Surface Involving the M20 Loop Region, J. Med. Chem. 49 (24) (2006) 6977–6986.

[30] M.L. Dennis, M.D. Lee, J.R. Harjani, M. Ahmed, A.J. DeBono, N.P. Pitcher, Z.-C. Wang, S. Chhabra, N. Barlow, R. Rahmani, B. Cleary, O. Dolezal, M. Hattarki, L. Aurelio, J. Shonberg, B. Graham, T.S. Peat, J.B. Baell, J.D. Swarbrick, 8-Mercaptoguanine Derivatives as Inhibitors of Dihydropteroate Synthase, Chem. – A Eur. J. 24 (8) (2018) 1922–1930.

[31] R. Abagyan, M. Totrov, Biased Probability Monte Carlo Conformational Searches and Electrostatic Calculations for Peptides and Proteins, J. Mol. Biol. 235 (3) (1994) 983–1002.

[32] M. Ikram, A. Haider, M. Imran, J. Haider, S. Naz, A. Ul-Hamid, W. Nabgan, M. Mustajab, A. Shahzadi, I. Shahzadi, M.A. Raza, G. Nazir, Facile synthesis of starch and tellurium doped SrO nanocomposite for catalytic and antibacterial potential: In silico molecular docking studies, Int. J. Biol. Macromol. 221 (2022) 496–507.

[33] C. Krishnaraj, P. Muthukumaran, R. Ramachandran, M.D. Balakumaran, P. T. Kalaichelvan, Acalypha indica Linn: Biogenic synthesis of silver and gold nanoparticles and their cytotoxic effects against MDA-MB-231, human breast cancer cells, Biotechnol. Rep, 4 (2014) 42–49.

[34] W. Li, G. Cai, P. Zhang, A simple and rapid Fourier transform infrared method for the determination of the degree of acetyl substitution of cellulose nanocrystals, J. Mater.Sci 54 (10) (2019) 8047–8056.

[35] E. Umar, M. Ikram, A. Haider, A. Shahzadi, A. Ul-Hamid, Improved catalytic and bactericidal behavior with in silico molecular docking analysis of barium/chitosan doped tungstate oxide nanoplates, Surf. Interfaces 38 (2023), 102835.

[36] M.A. Subhan, T.P. Rifat, P. Chandra Saha, M.M. Alam, A.M. Asiri, M.M. Rahman, S. Akter, T. Raihan, A.K. Azad, J. Uddin, Enhanced visible light-mediated photocatalysis, antibacterial functions and fabrication of a 3-chlorophenol sensor based on ternary Ag2O·SrO·CaO, RSC Adv. 10 (19) (2020) 11274–11291.

[37] F. El-Sayed, M.S.A. Hussien, T.H. AlAbdulaal, A.-H. Abdel-Aty, H.Y. Zahran, I. S. Yahia, M.S. Abdel-wahab, E.H. Ibrahim, M.A. Ibrahim, H. Elhaes, Study of catalytic activity of G-SrO nanoparticles for degradation of cationic and anionic dye and comparative study photocatalytic and electro & photo-electrocatalytic of anionic dye degradation, J. Mater. Res. Technol. 20 (2022) 959–975.

[38] M.A. Ashraf, W. Peng, Y. Zare, K.Y. Rhee, Effects of Size and Aggregation/Agglomeration of Nanoparticles on the Interfacial/Interphase Properties and Tensile Strength of Polymer Nanocomposites, Nanoscale Res. Lett. 13 (1) (2018) 214.

[39] M. Ikram, T. Inayat, A. Haider, A. Ul-Hamid, J. Haider, W. Nabgan, A. Saeed, A. Shahbaz, S. Hayat, K. Ul-Ain, A.R. Butt, Graphene Oxide-Doped MgO Nanostructures for Highly Efficient Dye Degradation and Bactericidal Action, Nanoscale Res. Lett. 16 (1) (2021) 56.

[40] S.A. Bhat, N. Rashid, M.A. Rather, S.A. Bhat, P.P. Ingole, M.A. Bhat, Highly efficient catalytic reductive degradation of Rhodamine-B over Palladium-reduced graphene oxide nanocomposite, Chem. Phys. Lett. 754 (2020), 137724.

[41] S.K. Jesudoss, J.J. Vijaya, L.J. Kennedy, P.I. Rajan, H.A. Al-Lohedan, R. J. Ramalingam, K. Kaviyarasu, M. Bououdina, Studies on the efficient dual performance of $Mn1–xNixFe_2O_4$ spinel nanoparticles in photodegradation and antibacterial activity, J. Photochem. Photobiol. B Biol. 165 (2016) 121–132.

[42] G.R. Navale, C.S. Rout, K.N. Gohil, M.S. Dharne, D.J. Late, S.S. Shinde, Oxidative and membrane stress-mediated antibacterial activity of WS_2 and rGO-WS_2 nanosheets, RSC Adv. 5 (91) (2015) 74726–74733.

[43] M. Ikram, I. Hussain, J. Hassan, A. Haider, M. Imran, M. Aqeel, A. Ul-Hamid, S. Ali, Evaluation of antibacterial and catalytic potential of copper-doped chemically exfoliated boron nitride nanosheets, Ceram Int 46 (13) (2020) 21073–21083.

[44] M. Ikram, E. Umar, A. Raza, A. Haider, S. Naz, A. Ul-Hamid, J. Haider, I. Shahzadi, J. Hassan, S. Ali, Dye degradation performance, bactericidal behavior and molecular docking analysis of Cu-doped TiO_2 nanoparticles, RSC Adv. 10 (41) (2020) 24215–24233.